12 Solid State Quantum Computers

12.1 Spins in semiconductor structures

12.1.1 Spins in solids

Some solid state implementations of spin-qubits may be considered direct extensions of liquid state NMR: Kampermann and Veeman used a quadrupolar system [291], much like a similar system in a liquid crystal [292]. The main difference between NMR in solids and NMR in liquids is the lack of motion. When nuclear spins are located at fixed positions in solids, they are subject to some interactions that are averaged out by the molecular motion in liquids. This includes the quadrupole interaction between the nuclear quadrupole moment and the electric field gradient as well as the magnetic dipole-dipole couplings, which are much stronger than the scalar couplings used in liquid-state NMR. Typical values of dipole coupling constants are in the kHz range rather than the Hz-range relevant for J-couplings in liquids. This results in correspondingly faster gate operations (μs rather than ms). However, dipolar couplings exist not only between the qubits, but also between qubits and environment, resulting in correspondingly faster decoherence.

A scheme that is intermediate between liquid state NMR and the single-spin solid state NMR approach is the "crystal-lattice quantum computer" [293, 294, 295], where arrays of identical nuclear spins are used as a single qubit. Compared to liquids, these solids offer the possibility of increasing the spin polarization, not only by lowering the temperature, but also by polarization transfer from electronic spins, e.g., by dynamic nuclear polarization. Addressability of individual qubits could be obtained by a strong field gradient produced by a micrometer-sized ferromagnet. Furthermore, solids are required for some detection schemes that offer higher sensitivity than the usual inductive detection [296].

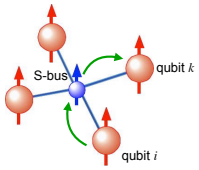

Figure 12.1: System for coupling 4 nuclear spins (red) via an electron spin (blue).

A potentially more powerful scheme was demonstrated by Mehring *et al.* [297]. As shown in figure 12.1, their system used an electron spin coupled to different nuclear spins by hyperfine interaction. They also introduced the idea of using electron spins as "bus-qubits" to allow nuclear spins to efficiently exchange information.

12.1.2 ^{31}P in silicon

A nuclear spin qubit that can be combined with single-spin detection was proposed by Bruce Kane[298]. He suggested to use the spins of ^{31}P impurities in Si, the only $I = 1/2$ shallow (group V) donor in Si. The ^{31}P:Si system was exhaustively studied around 1960 [299] in the first electron-nuclear double-resonance experiments. At sufficiently low ^{31}P concentrations at temperature $T = 1.5$ K, the electron spin relaxation time is thousands of seconds and the ^{31}P nuclear spin relaxation time exceeds 10 hours. This system would therefore allow for a large number of gate operations within a decoherence time.

Figure 12.2 shows the principle of this scheme: the ^{31}P atoms are to be placed in a matrix of ^{28}Si (which has no nuclear spin). Single-qubit operation on these qubits could be similar to those of NMR systems, i.e., by resonant radio-frequency

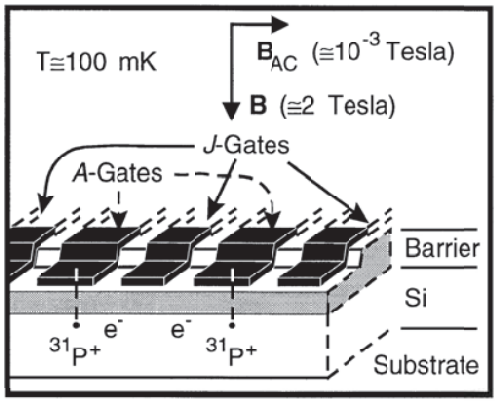

Figure 12.2: Proposed scheme for a quantum computer that uses ^{31}P atoms in a ^{28}Si matrix [298].

pulses. However, since all qubits share the same chemical environment, their resonance frequencies are identical. Addressing them would thus require local control schemes. Kane's proposal was to use small electrodes, which are labeled "A-gates" and "J-gates", respectively, in Fig. 12.2. The electric fields applied through these electrodes would couple to the charge of the impurity electron and indirectly affect the nuclear spin resonance frequency. So the electron spins of the dopants would play an important role, similar to the S-bus concept.

12.1.3 The qubit system

The P-donor system contains two spins: the electron spin ($S = 1/2$) and the ^{31}P nuclear spin (I=1/2). The Hamiltonian of the two spins interacting with the external magnetic field and with each other can be written as

$$\mathcal{H} = \Omega_S S_z - \Omega_I I_z + A I_z S_z.$$

Here, the first two terms represent the Zeeman interaction of the electron and nuclear spin, respectively. The third term is the hyperfine coupling between the two spins.

As shown in figure 12.3, the four eigenstates of this system are $|\downarrow\uparrow\rangle$, $|\downarrow\downarrow\rangle$, $|\uparrow\downarrow\rangle$, and $|\uparrow\uparrow\rangle$, where the first position refers to the electron and the

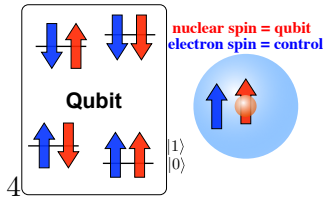

Figure 12.3: States of the electron-nuclear spin system in Kane's proposed qubit.

second to the nuclear spin state. Their energies are

$$\mathcal{E}_{\downarrow\uparrow} = \frac{-\Omega_S - \Omega_I}{2} - \frac{A}{4} \qquad \mathcal{E}_{\downarrow\downarrow} = \frac{-\Omega_S + \Omega_I}{2} + \frac{A}{4}$$
$$\mathcal{E}_{\uparrow\downarrow} = \frac{\Omega_S + \Omega_I}{2} - \frac{A}{4} \qquad \mathcal{E}_{\uparrow\uparrow} = \frac{\Omega_S - \Omega_I}{2} + \frac{A}{4}.$$

The hyperfine coupling constant A between electrons and nuclei depends on the electron density $|\Psi|^2$ at the site of the nucleus. If the voltage applied to the gate electrodes changes the electrostatic potential near the donor sites, it shifts the electrons closer or farther from the gates and thereby changes the electron density at the site of the nucleus and therefore its hyperfine coupling. Kane's proposal uses this possibility to tune the resonance frequency of the qubit. For this purpose, it uses a two-dimensional subspace of the 4-dimensional Hilbert space of the ^{31}P electron-nuclear spin system: the electron spin is fixed in the $|\uparrow\rangle$-state, while the nuclear spin represents the qubit. The two qubit states are thus

$$|0\rangle = |\downarrow\uparrow\rangle, \quad |1\rangle = |\downarrow\downarrow\rangle$$

and their energies $(-\Omega_S - \Omega_I)/2 - A/4$ and $(-\Omega_S + \Omega_I)/2 + A/4$. For this two-dimensional subspace, we can write an effective Hamiltonian

$$\mathcal{H}_2 = (\frac{A}{2} - \Omega_I) I_z.$$

Adjusting the hyperfine constant A therefore adjusts the transition frequency of the qubit.

The electrodes labelled "A-gates" could therefore be used for addressing the individual qubits by shifting their energies in and out of resonance. As shown in figure 12.4, gate voltages of $\approx 0 - 1$

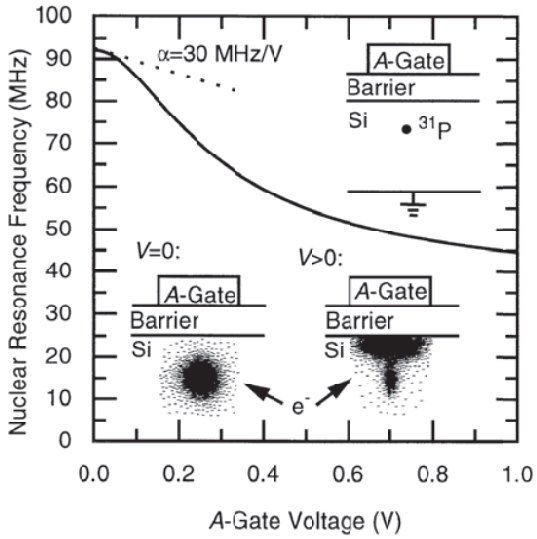

Figure 12.4: Dependence of the hyperfine coupling constant on the gate voltage, according to [298].

V should be able to tune the nuclear spin Larmor frequency between 50 and 100 MHz. Similarly J-gates would move electron density between the donor sites (see Fig. 12.6), thus inducing an indirect coupling between qubits and allowing the addressing of pairs of qubits.

The Kane proposal has a number of very attractive features. In particular, the long relaxation times of both spins in the system indicate the possibility of performing many gate operations before decoherence leads to the loss of quantum information. The reason for these long decoherence times can be traced to the fact that ^{28}Si, which forms the main component of natural abundance silicon, has no nuclear spin. Accordingly, it does not perturb the electron spin by hyperfine interaction. The effect of the 4.6% natural abundance ^{29}Si can be reduced by isotopic enrichment. Since the nuclei involved are relatively light, spin-orbit interaction is weak, which also contributes to the long decoherence times. While the manufacturing poses significant challenges, the enormous investments of the semiconductor industry in technological developments of Si-based circuits has led to a highly advanced technology base for this system.

12.1.4 Qubit operations

To meet the di Vincenzo criteria, it is necessary to initialize the qubits. This cannot be done by simply cooling the system to the ground state: The Boltzmann factor for electron spins at a temperature of 0.1 K, in a magnetic field of 2 T, is close to 1. For the nuclear spins under the same condition is $\approx 5 \cdot 10^{-3}$ - clearly too low for initialization of the qubit into the ground state.

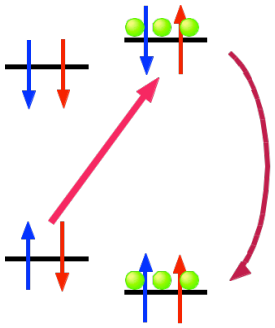

Figure 12.5: Initialization of the ^{31}P qubit. Blue is the electron spin, red the nuclear spin.

While thermal polarization is not sufficient to initialize the nuclear spin qubit, it can be used to initialize the electron spin. From the state, where both qubit states are equally populated, initialization into the ground state can be achieved by transferring the spin polarisation from the electron to the nuclear spin. For this purpose, a microwave pulse inverts the transition between the $|\uparrow\downarrow\rangle \leftrightarrow |\downarrow\uparrow\rangle$ states, as shown in figure 12.5. From this state, thermal relaxation will primarily populate the $|\uparrow\uparrow\rangle$ state, thus enhancing the population of the $|0\rangle$ state of the qubit. The remaining population, which decays into the $|1\rangle$ state of the qubit, can be excited again, until the vast majority of the atoms have accumulated in the logical ground state.

While thermal relaxation is a suitable way of initializing a qubit before a calculation, it is usually too slow for use in repetitive error correction. In the case of the Kane system, alternative initialization schemes are being explored, such as

- Optical spin injection through SiGe super-

lattices or quantum dots

- Electrical spin injection
- Readout: reading the current state of the spin (→ 12.1.5) and applying a NOT gate if required.

Single-qubit gate operations can be driven by radio-frequency (RF) fields. The external control fields generally drive all qubits of the sample, but they only have an effect on those qubits whose transition frequency is shifted into resonance with the applied RF frequency.

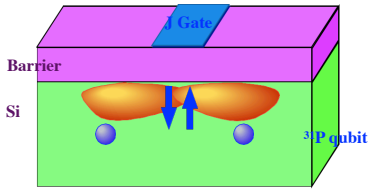

Figure 12.6: Principle of operation of J-gates.

While each A-gate operates on the transition frequency of an individual qubit, the J-gates are designed to affect primarily the interaction between two qubits. For this purpose, it draws electron density of both neighboring qubits into the region between them. The resulting overlap between the two electron densities results in a spin-dependent exchange interaction. Through the hyperfine interactions of both qubits, this also mediates an effective exchange interaction between the nuclear spin qubits. The strength of this interaction is of the order of 75 kHz.

12.1.5 Readout

Another requirement is the detection of the individual spins. Since the first proposal, a number of schemes have been developed and tested for this purpose. They all involve some conversion of the nuclear spin qubit states to electronic states. One possible scheme uses, in addition to the nuclear spin and its associated electron spin, an additional readout electron.

The 2-electron spins interact with a given magnetic field such that, in the absence of an interaction between them, their energies are given

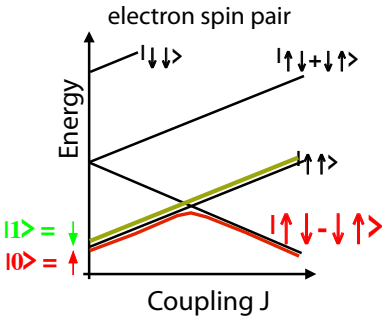

Figure 12.7: Conversion of the logical $|0\rangle$ state to the electronic singlet state.

by their Zeeman interaction, as shown on the left-hand side of figure 12.7. Both electron spins must be fully polarized into the $|\uparrow\uparrow\rangle$ state. Using a J-gate, the interaction between the electrons is slowly turned on. When the coupling strength becomes equal to the Zeeman interaction, the $|\uparrow\uparrow\rangle$ state becomes degenerate with the singlet state $|\uparrow\downarrow\rangle - |\downarrow\uparrow\rangle$. For even stronger J coupling, the singlet state becomes the ground state. This crossing can be adiabatic, with the system remaining in the ground state, or non-adiabatic, with the electron spin pair remaining in the $|\uparrow\uparrow\rangle$ state.

Considering in addition the nuclear spin, the hyperfine interaction makes the states near the energy level crossing dependent on the nuclear spin. If the nuclear spin is in $|\uparrow\rangle$ (the logical $|0\rangle$ state), the system avoids the crossing of energy levels[1] and remains in the overall ground state. If the nuclear spin is $|\downarrow\rangle$, the corresponding states cross and the system ends up in the $|\uparrow\uparrow\rangle$ triplet state of the two electrons.

The singlet state can then be converted into a charge state, by transferring the electron to the readout donor. For a suitably polarized additional electron spin, this is only possible for the singlet state, but not for the triplet state. The charge state can then be detected via a single electron transistor [298, 300].

In a related experiment, the signature of a sin-

[1] under adiabatic conditions

gle ^{31}P nuclear spin was measured in a Si-FET [301]. In a slightly different system, the coherent evolution of an ensemble of ^{31}P nuclear spins was measured [302]. It remains to combine the coherent evolution with the single spin detection.

A major challenge to the Kane proposal remains the precise implantation of the P-donors with a precision of a few nanometers. Several projects working towards this goal use scanning probe microscopy for identifying the target position. One possibility may be to implant ions through the tip of an AFM, which contains a nanometer-sized hole. A second approach is to use an STM tip to selectively remove hydrogen atoms from an H-terminated silicon surface. The unprotected bond can then bind to PH_3 molecules which may then be overgrown by an additional Si layer [303, 304].

12.1.6 Si/Ge heterostructures

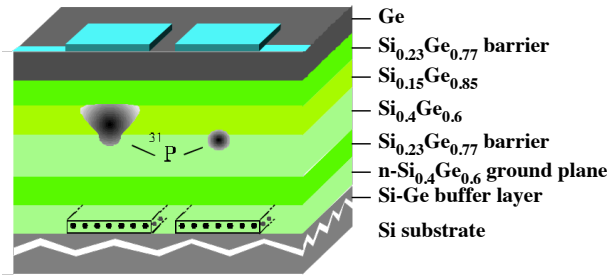

Figure 12.8: A proposal for a ^{31}P qubit on the basis of a SiGe heterostructure.

The concept of using donor atoms in silicon as qubits has also been used in different settings. Figure 12.8 shows one concept based on Si/Ge heterostructures [305]. An attractive feature of such heterostructures is that the electron spin Larmor frequency can be tuned by band-gap engineering and by applying electrical fields.

The Larmor frequency of an electron spin is

$$\Omega_L = \frac{g\mu_B}{\hbar} B,$$

where B is the flux density,

$$\mu_B = \frac{e\hbar}{2m_e} = 9.27 \cdot 10^{-24} \frac{\mathrm{J}}{\mathrm{T}}$$

is the Bohr magneton and g is the $g-$factor. For free electrons, it is close to 2, in condensed matter, it can vary over a significant range of positive and negative values of order unity. If the $g-$factor of the donor spin can be modulated, it can be moved into- and out of resonance.

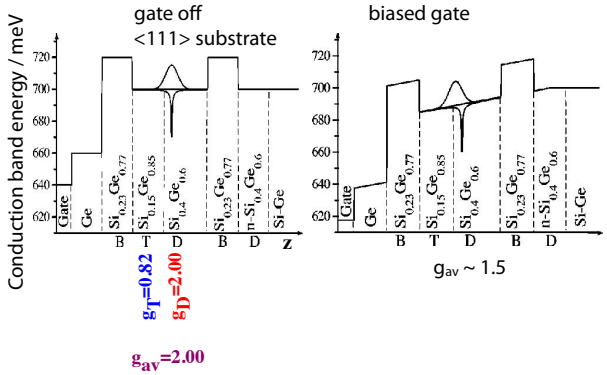

Figure 12.9: Proposed Si/Ge heterostructure with different g-factors, depending on gate potential.

The basic idea is to use different types of SiGe compositions with different g-factors, as shown in fig. 12.9. Using electrodes, the electrons can be pushed into different materials, thereby changing their resonance frequency and providing addressability for single-qubit gates. For this purpose, the defect must be positioned in $Si_{0.4}Ge_{0.6}$, where the electronic g-factor is close to 2. In the neighboring layer consisting of $Si_{0.15}Ge_{0.85}$, the g-factor is of the order of 0.82. If a suitable field is applied, which lowers the potential of the $Si_{0.15}Ge_{0.85}$ layer, the electronic wave-function is partially pushed over into that layer and the effective g-factor is lowered correspondingly, to an estimated value of 1.5.

The overlap of the wave function with the $Si_{0.15}Ge_{0.85}$ also changes the Bohr radius and thereby affects the overlap of the electron with neighboring electrons. The gate therefore also has the function of the J-gate, making the implementation of separate J-gates unnecessary.

12.1.7 Schemes with tunable qubit-qubit interactions

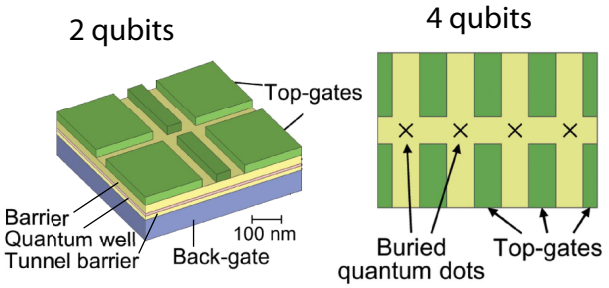

Figure 12.10: Electrostatically confined electron qubits in a Si/SiGe quantum well.

Friesen [306] goes into another direction: he proposed to define the qubits by electrostatic confinement of electrons in Si / SiGe quantum wells. Figure 12.10 shows two possible structures for 2 and 4 qubits.

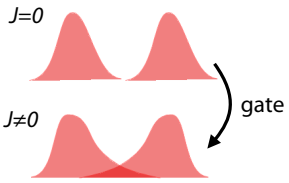

Figure 12.11: Change of overlap between two electron wave packets.

Since the Bohr radius of the electron can be changed by applying potentials to the electrodes, it becomes possible to create non-vanishing overlaps between the wave functions of neighboring electrons, as shown in figure 12.11. The overlap determines the exchange interaction between the electrons:

$$\mathcal{H}_J = J\vec{S}_1 \cdot \vec{S}_2.$$

This allows for switchable interactions, which are essential for 2-qubit gates.

Using donors in silicon may not require patterning on the nm scale. Using random doping and tailored optical excitation, it may be possible to control at least small groups of qubits [307]. In this proposal, the qubits would be the spin states of deep donors, like Si:Bi. An additional control impurity, e.g. Er, would be excited by a suitable laser. Depending on its electronic state, its wavefunction would overlap with the qubits and thereby mediate a coupling between them. This proposal obviously requires a significant amount of fine-tuning for every qubit and control impurity. However, to some degree such fine tuning will be required for every nano-fabricated device, since the parameters of every artificial structure vary to some degree.

12.2 Spin centers

In this section, we consider spin qubits in different solid-state environments.

12.2.1 N@C60

As discussed in section 11.5, neutral atoms are very attractive qubits, with potentially long lifetimes and strong interactions. One difficulty is that most atoms are unstable if they are not well isolated. As an example, nitrogen atoms are mostly bound in N_2 molecules. Using them as qubits therefore requires some way of isolating them from each other.

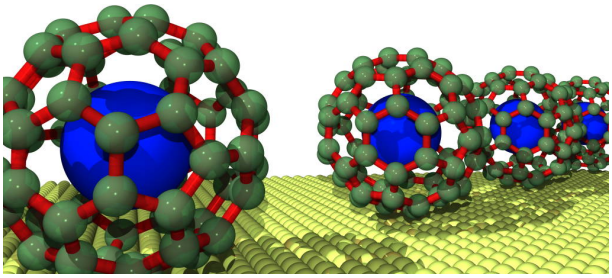

Figure 12.12: Array of N@C60 molecules forming a quantum register.

This can be achieved, e.g., with endohedral fullerenes N@C_{60} and P@C_{60} [308]. The endohedral atom is trapped inside the highly symmetric fullerene molecule, which can be considered a nanometer-sized trap for a neutral atom. The nitrogen atom has an electron spin of S=3/2, while

the nucleus has spin I=1 (for ^{14}N or I=1/2 for ^{15}N and ^{31}P). In the context of quantum computing, the main interest in them arises from the possibility to use them as room-temperature, nanometer-sized traps for neutral atoms [309]. In particular, nitrogen and phosphorous atoms are attractive candidates, which are hard to trap with other methods. Their p-shell is half full, which results in a total electron spin $S = 3/2$. The electron spin is coupled to the nuclear spin by hyperfine interaction. The relevant Hamiltonian of the spin system can be written as

$$\mathcal{H} = g\mu_B \vec{B}_0 \cdot \vec{S} - \gamma_n \vec{B}_0 \cdot \vec{I} + A\vec{S} \cdot \vec{I}. \quad (12.1)$$

Here, $\vec{S}$ is the electron spin, $\vec{I}$ the nuclear spin, g, μ_B and γ_n are the electron g-factor, Bohr's magneton and the nuclear gyromagnetic ratio, $\vec{B}_0$ is the magnetic field and A the hyperfine coupling constant. For the atoms trapped in a C_{60} molecule, the corresponding values are

nucleus	spin / $\hbar$	A/MHz
^{14}N	1	15.88
^{15}N	1/2	22.26
^{31}P	1/2	138.4

Using the electronic as well as the nuclear spin degrees of freedom allows one, in principle, to encode up to three qubits in each molecule.

Fig. 12.12 shows a possible use of these molecules as qubits: each C60 molecule acts as a trap for a nitrogen or phosphorus atom, whose spins encode the quantum information. The major properties that make this system so attractive for quantum information processing is that (i) the spins have very long lifetimes, with the longitudinal relaxation time T_1 exceeding 1s at low temperature [310] and (ii) they are easier to manipulate than dopant atoms inside semiconductors. It would be possible, e.g., to deposit them on the surface of a suitable material, such as silicon, and manipulate them by a scanning tunneling microscope [311].

12.2.2 Addressing and gate operations

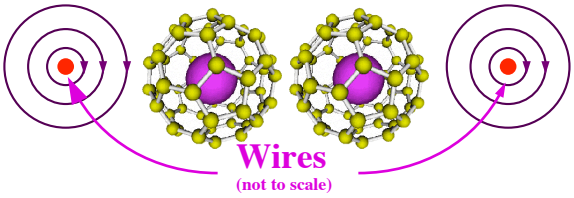

Figure 12.13: Scheme for resonant addressing of N@C60 molecular spins: the wires cary copropagating currents, which generate a magnetic field gradient superimposed over a static external magnetic field.

Gate operations can be performed by resonant microwave pulses applied to the electron spins and radio-frequency pulses applied to the nuclear spin transitions [312]. Addressing of the individual molecules can be achieved, e.g., by applying a magnetic field gradient that shifts the resonances of the individual molecules [313]. By depositing copper wires on the Si surface and running currents of the oder of 1 A through two parallel wires generates a magnetic field that combines with the homogeneous background magnetic field to a magnetic field gradient between the two wires, as shown schematically in Fig 12.13.

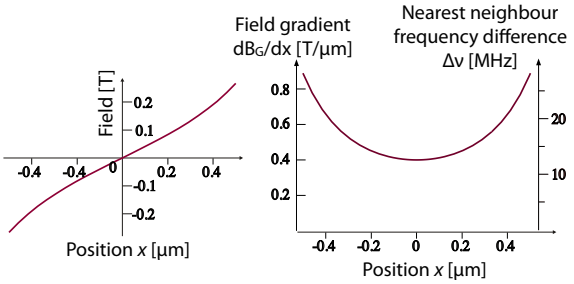

Figure 12.14: Magnetic field, field gradient and frequency difference between adjacent N@C_{60} qubits as a function of position.

For a distance between the wires of the order of 1 μm, the resulting gradient would be of the order

of 4×10^5 T/m. For two N@C60 molecules separated by 1.14 nm (the diameter of the molecules), this results in a frequency splitting of 12.7 MHz. This should allow precise qubit addressing in frequency space. If larger distances are chosen between the molecules, the frequency difference is correspondingly larger.

The implementation of 2-qubit gates requires interactions between the qubits. A readily available interaction is the dipole-dipole coupling, whose coupling constant is

$$d = \frac{\mu_0}{4\pi} \frac{\gamma_1 \gamma_2}{r^3} (3\cos^2\theta - 1),$$

with γ_i representing the gyromagnetic ratio of the spins, r the distance between them and θ the angle between the vector connecting them and the direction of the magnetic field. For N atoms at a distance of 1.1 nm, the coupling strength reaches about 50 MHz, which is sufficient for gate times of the order of 10 ns.

12.2.3 Gated couplings

One major difficulty of the system is that the magnetic dipole couplings between the molecules are static, i.e. they cannot be switched as required by the algorithms. This problem can be solved by using the electron and nuclear spin for encoding a single logical qubit.

Figure 12.15 shows the relevant energy level scheme for the the ^{15}N@C60 or ^{31}P@C60 electron-nuclear spin system under the Hamiltonian (12.1). The arrows label the allowed magnetic dipole transitions of the electron (vertical arrows) and the nuclear spin (horizontal arrows).

The four nuclear spin transitions and the electron spin transitions are split by the hyperfine coupling of 22 MHz (^{15}N) or 138 MHz (^{31}P). Using both degrees of freedom allows one to store the information in the nuclear spin degree of freedom. Since the nuclear spin couples only weakly to other degrees of freedom, the quantum information stored in it has a long lifetime. It is also effectively isolated from the other molecules,

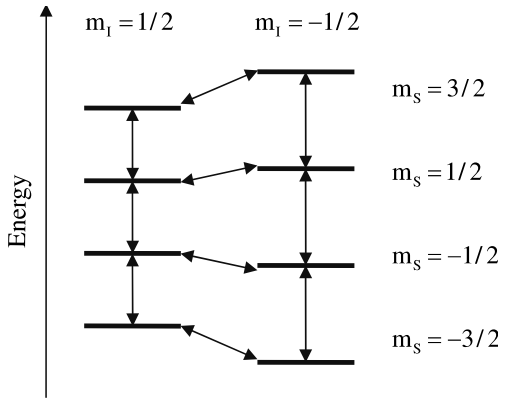

Figure 12.15: Energy levels of the ^{15}N@C60 or ^{31}P@C60 electron-nuclear spin system. I refers to the nuclear spin, S to the electron spin.

since the magnetic dipole-dipole couplings between the nuclear spins is $\approx 10^9$ times smaller than that between the two electron spins.

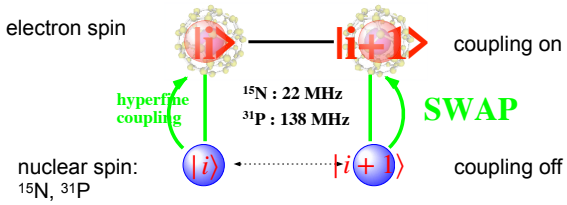

Figure 12.16: The dipole-dipole interaction between neighboring molecules can be switched on (off) by flipping the qubits from the nuclear to the electron spin (from the electron to the nuclear spin).

When the algorithm requires an active coupling between two qubits, it can be generated by using the large difference between the interactions between 2 nuclear spins vs. 2 electron spins: the ratio of the coupling strengths is of the order of 10^9. If the qubits are stored in the nuclear spin degrees of freedom, there is therefore effectively no interaction. When an interaction is required, the qubits can be transferred into the electron spin degrees of freedom, thereby switching the coupling on (→ Figure 12.16). The two-qubit operation is then performed on the electron

spins and the qubits are switched back to the nuclear spins when the gate operation is complete [313, 309, 314].

12.2.4 Single-Spin Readout

While several elements of this scheme have been tested, the readout of the qubits remains a significant challenge. Experimental evidence [315] shows that it is possible to electrically contact individual magnetic N@C60 molecules and measuring spin excitations in their electron tunneling spectra. The tunneling spectra allow the identification of the charge and spin states of the molecule. If such measurements can be combined with the other elements, a quantum computer based on endohedral fullerenes appears possible.

Another experimental approach to single-spin detection uses a scanning tunneling microscope (STM) [316, 317, 318]. While the details of the experiment must be considered unknown, it appears that the tunneling current contains an oscillating component at the Larmor frequency if the tip is placed over a paramagnetic molecule. The oscillating signal component is separated from the dc component and fed into a microwave spectrum analyzer.

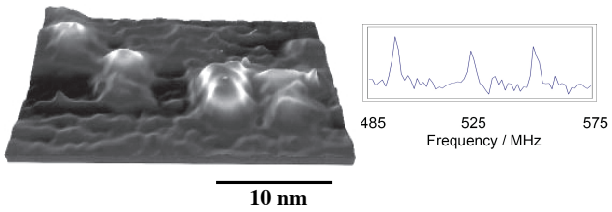

Figure 12.17: Spatial distribution of STM-EPR signal on graphite surface. The elevated regions correspond to four adsorbed BDPA molecules. The right-hand part of the figure shows the STM-detected EPR spectrum of TEMPO clusters. The three resonance lines are due to the hyperfine interaction with the ^{14}N nuclear spin [318].

By setting the detection frequency to the EPR frequency, it is possible to map the spin density on the surface. The example shown in Figure 12.17 represents the signal from four organic radical molecules (BDPA) that were deposited on a graphite surface [318]. The right-hand part shows the STM-detected EPR signal from TEMPO molecules, another stable radical. In this case, the electron spin couples to the ^{14}N nuclear spin. The hyperfine interaction splits the EPR resonance into three resonance lines, corresponding to the three nuclear spin states. A related technique is the mechanical detection of magnetic resonance [319], which has been shown to be capable of single-spin detection in suitable systems [320].

The most powerful techniques for measuring magnetic resonance transitions of single spins are based on optical measurements. This will be discussed in the context of the NV center in diamond, in section 12.3.

Both techniques – optical and scanning probe microscopy – allow for the detection of individual electronic spins. While this is not a readout of the spin state, it can be used as such if the spin being detected is not the qubit to be read out, but coupled to the computational qubit: the coupling shifts the EPR frequency, allowing one to detect the spin state of the computational qubit through the EPR frequency of the readout qubit.

A difficulty of the optical readout is that the spatial resolution is limited by the optical wavelength. Near-field optical techniques reach better spatial resolution, but their collection efficiency is too low for efficient readout of qubit states. STM-based systems require mechanical motion, resulting in a slow readout process. For an all solid state system, electronic readout would provide the possibility to eliminate external optical and mechanical (STM) accessories. A possible approach is to use single electron transistors (SET's), in combination with spin-dependent tunneling processes [321, 322], but their viability for single-spin readout depends on the specific parameters of the system.

12.2.5 Rare Earth Ions

The electronic properties of rare earth ions, i.e. the elements from Lanthanum ($Z = 57$) to to Lutetium ($Z = 71$) distinguish them from almost all other elements. The states that are responsible for these special properties are the partly filled $4f$ orbitals. The relevant transitions that fall into the visible or near-IR range of the spectrum are all forbidden by parity and often also by spin selection rules. This results in long lifetimes and narrow natural line widths [323, 324]. The emission wavelengths of different elements cover a large wavelength range in the near UV, visible as well as the infrared region. They are therefore often used for tuning the emission characteristics of light sources.

Due to the shielding, the states are only weakly affected by crystal field effects, which results in relatively small inhomogeneous broadening. These properties have fascinated physicists working in atomic spectroscopy as well as physicists and engineers interested in optical data storage [325] or optical data processing [326].

Rare earth ions were also found to be useful qubits for quantum information processing (see, e.g., [327, 328]), either stored in electromagnetic traps [329] or as dopant ions in dielectric crystals [330]. Compared to many other solid-state systems, they can be operated at relatively "warm" temperatures close to 4.2 K. The optical as well as the magnetic dipole degrees of freedom offer many possibilities for generating gate operations.

An additional use for rare earth ions in solid materials came with the search for quantum memories [331][332]. This aspect is discussed in section 12.2.6.

The materials used for this purpose are mostly based on Pr^{3+} or Eu^{3+} substituting for La^{3+} or Y^{3+}, such as $Pr{:}La_2(WO_4)_3$, $Pr{:}YAlO_3$, $Pr{:}Y_2SiO_5$, or $Eu^{3+}{:}Y_2SiO_5$. Relevant criteria include the accessibility of suitable transition frequencies by available lasers, the linewidth of these transitions, the lifetimes of the electronic and nuclear spin states, the transition strengths and absorption depths for a given amount of doping. High levels of doping can generate stress in the crystal and therefore broadening of the resonance lines, in particular if the ionic radii of the host and guest ion differ significantly.

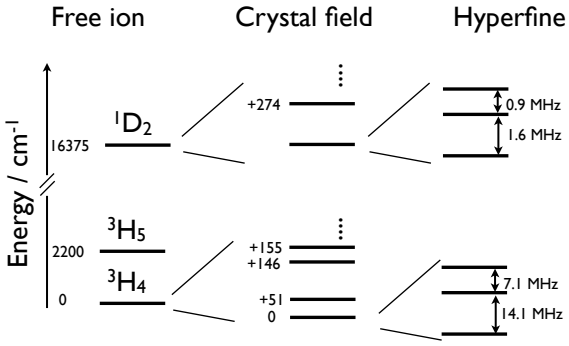

Figure 12.18: Energy levels of the Pr^{3+} ion substituting for Y^{3+} in $YAlO_3$.

Fig. 12.18 shows, as a typical example, the simplified energy level scheme of the Pr^{3+} ion substituting for Y^{3+} in an $YAlO_3$ crystal. Among the many possible optical transitions, that between the $^3H_4$ electronic ground state and the $^1D_2$ electronically excited state is easily accessible by high-resolution ring dye lasers, with a transition energy of 16375 cm^{-1}, which corresponds to a wavelength of 610.7 nm. The highly degenerate states of the free ion split in the presence of a crystal field. At the same time, the crystal field also quenches the orbital angular momentum of the electrons.

On a much smaller energy scale, the states split further due to the hyperfine interaction and the interaction of the nuclear spin with external magnetic fields and the nuclear quadrupole moment with the electric field gradient tensor of the crystal. Both interactions are enhanced by the second-order hyperfine interaction. The ^{141}Pr nuclear spin shown in figure 12.18 has a value of 5/2.

12.2.6 Photonic quantum memories

In the context of quantum information, rare earth ions have been used as qubits in the form

of trapped ions. In solids, the main application is in the form of quantum memories, where qubits can be stored until they are needed - either for computing or for quantum communication (→ chapter 13).

These devices must store the complete quantum state of a photon in a suitable material for times of μs to s [333, 334]. For this purpose, it is necessary to convert 'flying qubits' into stationary qubits and vice versa. This is achieved when the photons interact with an optical transition. These processes can not only proceed directly, they can also be assisted by different experimental techniques, such as electromagnetically induced transparency (EIT) [335].

Compared to conventional optical storage, quantum memories require storage of the complete quantum state of a photon. This is nontrivial, since it is not possible to convert the quantum state into classical information; this is usually specified in terms of the "no-cloning theorem" Wootters and Zurek [56]. Quantum storage thus requires that not only the populations of the relevant states are conserved, but also the relative phases between them. This requirement is extremely difficult to meet in almost all solid-state materials, with crystals containing doped rare-earth ions as the major exception [336, 337, 331]: due to their electronic structure, the optical dephasing times are unusually long.

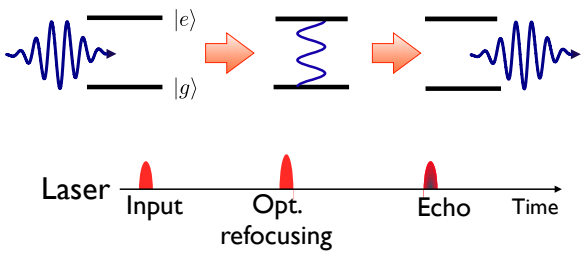

Figure 12.19: Photon echo as a short-time optical memory.

As illustrated in Fig. 12.19, the simplest optical storage scheme can be realized as a photon echo: The absorption process can be steered to implement a swap operation between the photon and the rare-earth ion qubits. It thus creates a superposition state of two electronic states $|g\rangle$ and $|e\rangle$, which contains the information about the quantum state of the absorbed photon, distributed over a large number of ions. Since the absorption probability of a single ion is quite low, this is usually done by letting the laser interact with an ensemble of N ions, so the resulting state is a superposition of $N-1$ ions in the ground state and one ion in the excited state.

The inhomogeneous broadening of the optical transition results in a dephasing of the information, which severely limits the storage time. Longer storage times can be achieved by reversing the dephasing, using a refocusing pulse to generate a photon echo. The photon echo corresponds to re-emission of the absorbed photon, in a direction which is determined by the directions of the incident pulse and the refocusing pulse.

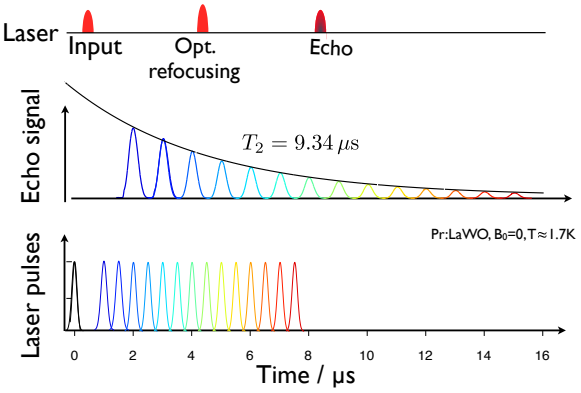

Figure 12.20: Experimentally measured photon echoes in Pr^{3+}:$La_2(WO_4)_3$ as a function of the delay between the pulses. The fitted curve corresponds to a dephasing time of $T_2 = 9.34\,\mu$s.

Figure 12.20 shows an example of photon echoes generated in Pr^{3+}:$La_2(WO_4)_3$, measured with a $\pi/2 - \tau - \pi - \tau$ sequence, as a function of the delay τ between the pulses. The decay of the echoes with increasing pulse separation can be fitted as an exponential decay $\propto e^{-4\tau/T_2}$ with a dephasing time $T_2 = 9.34\,\mu$s. This corresponds to the lifetime of quantum states in the electronic degrees of freedom for this material.

12.2.7 Nuclear spin storage

This simple photon echo experiment has several limitations: its efficiency is quite small - only a few percent of the incident light is typically recovered, the rest is lost to absorption, and the storage times are relatively short. Different solutions have been proposed for these problems [338, 339, 340, 331, 341], and a number of these improvements have been tested experimentally (see, e.g. [342, 343]). The ultimate goal is to store the state of a single photon with fidelity close to unity for times of the order of seconds to hours.

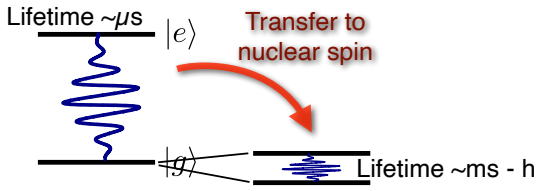

Figure 12.21: Transfer of coherence from optical to nuclear spin transition.

To increase the storage time, it is possible to transfer the information from the optical transition into the nuclear spin degree of freedom, as shown schematically in figure 12.21. This results in an extension of the lifetime by several orders of magnitude. Even more important, however, is that it now becomes easier to use established experimental techniques for further extending the lifetime. The main limitation for the decay of quantum information stored in the nuclear spin degrees of freedom of rare earth ions are the magnetic fluctuations of the environment. Their influence can be suppressed by different techniques, as discussed in section 7.6. The choice of techniques includes the application of suitable magnetic fields, which suppress the effect of magnetic field fluctuations on the transition frequency to first order [344], or by sequences of radio-frequency pulses that refocus the dephasing induced by the environment [345].

Fig. 12.22 shows some experimental data. The black curve in Fig. 12.22, labeled 'FID' shows the decay after the transfer from the electronic to

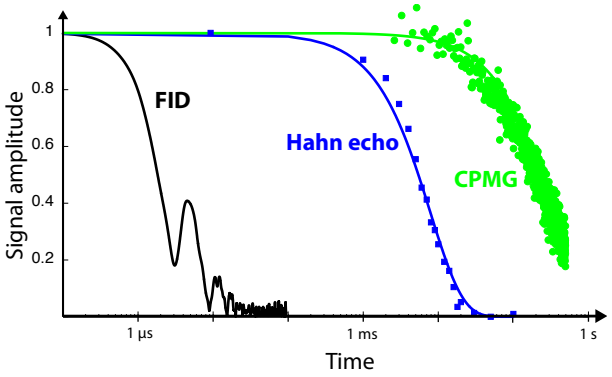

Figure 12.22: Increase of the lifetime of nuclear spin coherence by several orders of magnitude, using either Hahn echoes or the Carr-Purcell-Meiboom-Gill sequence.

the nuclear spin degrees of freedom. This decay is dominated by magnetic interactions and can be refocused either by a simple refocusing pulse ('Hahn-echo' in Fig. 12.20) or, more effectively, by a series of pulses (points labeled 'CPMG' in Fig. 12.22. Clearly, these refocusing techniques extend the lifetime of the coherence in the material by more than 5 orders of magnitude. Further extensions have been demonstrated in optimized material systems, up to storage times of the order of several hours [117, 346].

Rare earth ions can be used not only for information storage: once the information has been input into the system, it can also be processed by the usual quantum gate operations. Optical pulses as well as radio frequency fields can be used to generate the quantum logical gate operations.

12.2.8 Molecular Magnets

Molecules containing clusters of transition metal ions have also been proposed as possible qubit systems [347]. The ions in these "molecular magnets" are strongly coupled by exchange interaction and have large total spins. Examples include clusters like Mn_{12} [348, 349] shown in Figure 12.23 and Fe_8 [350] with total spin $S = 10$.

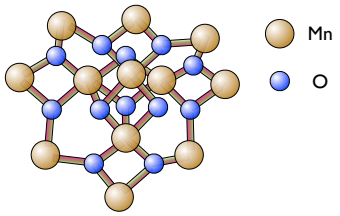

Figure 12.23: $Mn_{12}O_{12}$ cluster, forming the central part of a "molecular magnet" qubit.

The spin interacts with its anisotropic environment, resulting in a large zero-field splitting energy

$$\mathcal{H}_{ZF} = -D\,S_z^2,$$

which stabilizes the ground states with $m_S = \pm S$. In most cases, the environment does not have axial symmetry and the Hamiltonian therefore contains an additional anisotropy term,

$$\mathcal{H}_{ZF2} = -D\,S_z^2 - E\,\frac{1}{2}\left(S_+^2 + S_-^2\right).$$

If a magnetic field is applied along the z-axis, the total Hamiltonian becomes

$$\mathcal{H}_{mm} = -D\,S_z^2 - E\,\frac{1}{2}\left(S_+^2 + S_-^2\right) - \hbar\omega_L S_z. \quad (12.2)$$

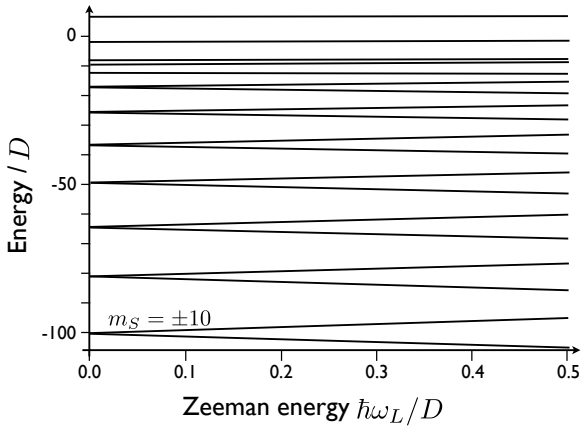

Figure 12.24: Energy levels of an $S = 10$ system, corresponding to the Hamiltonian (12.2), with $E/D = 0.05$.

As shown in Fig. 12.24, this completely lifts the degeneracy of the system. The $2S + 1$ energy levels offer a wide range of possible schemes for storing the quantum information in this system. However, since the energies are spread over a range of $> 100\,\mathrm{GHz}\,h$, it is an enormous challenge to implement coherent control for the complete system.

As an alternative, it was proposed to use only the two lowest energy levels, corresponding to $m_S = \pm S$. This does not eliminate the challenge of implementing coherent control, however, since these states are not directly coupled by a magnetic dipole transition.

A major challenge of these systems for quantum information applications is the coupling between the molecules and their environment, which leads to relatively fast decoherence, compared to the more rigid solid-state systems discussed above. For some systems, it is possible to deposit them as monolayers on a surface (often gold layers, see, e.g. [351]), without significantly changing their magnetic properties.

12.3 Color centers in wide-bandgap semiconductors

Apart from the properties of the actual qubits, their environment is also important for its usability. One class that has a range of useful properties are wide-bandgap semiconductors, specifically diamond and silicon carbide (SiC). Since their bandgap is > 2.5 eV, they are highly transparent in the visible wavelength range. They are also very robust, withstanding mechanical forces as well as high electrical fields and electromagnetic fields. The actual qubits are point-like defects in these crystals, which are often called color centers, i.e. point-like defects that can absorb and emit light at specific wavelengths.

While most solid-state qubit systems have to be operated at liquid-helium or even mK temperatures, these color centers typically can operate at room temperature.

12.3.1 The NV$^-$-center in diamond

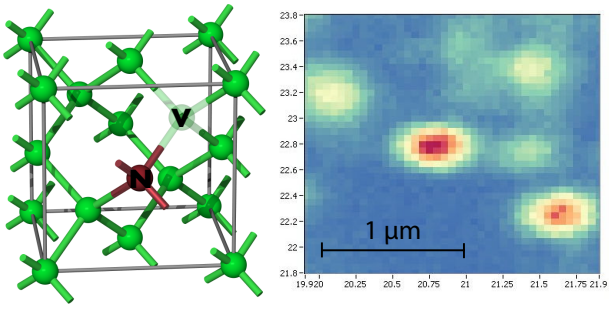

Figure 12.25: Structure of the N/V center in diamond. The right-hand side represents an image of a diamond surface, recorded by a scanning confocal microscope. Each bright spot represents a single N/V center.

Diamond has a number of well-characterized defects, of which the most prominent one is the nitrogen-vacancy center [352, 353]. As shown in figure 12.25, it consists of a nitrogen at a carbon site and an adjacent vacancy, i.e. a missing carbon. The defect contains a total of six electrons: two from a lone pair of the nitrogen pointing towards the vacancy, three from the dangling bonds of the carbons next to the vacancy plus an additional electron that generates the negative charge of the center. These electrons combine to a total spin $S = 1$.

The attractive properties of this center include the long coherence times at room temperature, and the special optical properties: the photostability is very high, allowing experiments on single centers for months without degradation of its properties.

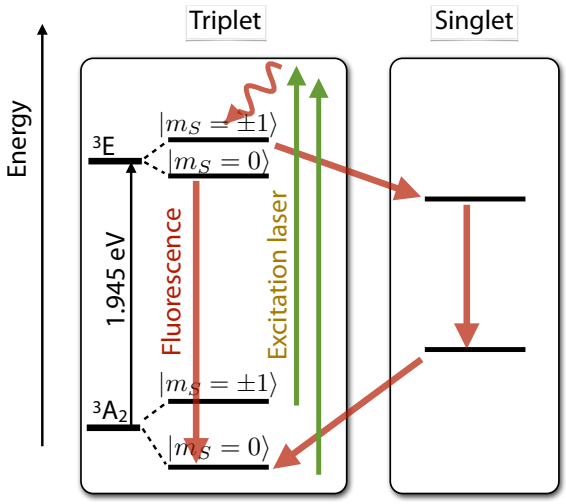

Figure 12.26: Relevant part of the electronic structure of the N/V center.

As shown in figure 12.26, the $^3A_2$ electronic ground state is connected by an optical transition to a ^3E electronically excited state. The zero-phonon line of this transition has a wavelength of $\lambda_0 = 637\,\text{nm}$. Initialization as well as readout of this qubit system rely on absorption-emission cycles between these two states. The phonon sidebands can be excited by green laser light (e.g. $\lambda = 532$ nm).

12.3.2 Initialization and readout

Between the two electronic triplet states are two singlet states, which can be populated by intersystem crossing processes. These processes are spin dependent, with the $m_S = \pm 1$ states having a significantly larger probability for crossing over into the single manifold. Pumping the system for $\approx 0.5\,\mu$s with < 1 mW of green laser light leaves it with high probability in the $m_S = 0$ spin state.

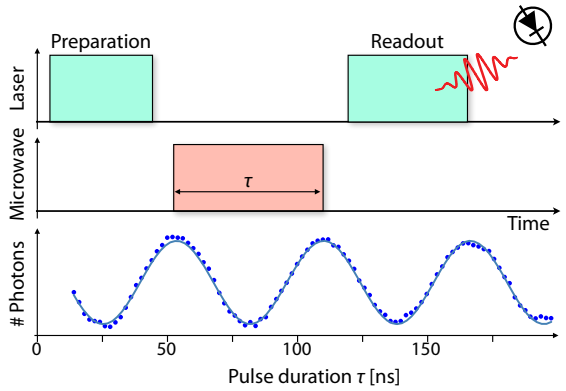

Figure 12.27: Initialization and readout of the electron spin.

The rate at which photons are scattered (absorbed and re-emitted) by the center depends on the spin state; it is significantly higher if the center is in the $m_S = 0$ state. This can be used to read out the spin state, as shown schematically in figure 12.27: An initial laser pulse brings the center into the $m_S = 0$ state. During the second laser pulse, photons are counted. If a microwave pulse is applied to the system during the period between the two laser pulses, it flips the spin between the $m_S = 0$ and the $m_S = \pm 1$ states. This is observed as an oscillation of the count rate, as shown in the bottom trace.

In the absence of a magnetic field, the $m_S = \pm 1$ spin states are degenerate, but separated from the $m_S = 0$ state by the zero field splitting of $D = 2.87$ GHz. A magnetic field lifts the degeneracy of the $m_S = \pm 1$ states. In addition, the electron spin is coupled to the nitrogen nuclear spin (usually ^{14}N, $I = 1$).

12.3.3 Nuclear spin interactions

Apart from the defects, diamond consists of carbon atoms, of which close to 99% are ^{12}C isotopes, which does not have a nuclear spin. However, 1.1 % are ^{13}C, which has a nuclear spin $I = 1/2$ and therefore interact with the electron. Their hyperfine coupling constant starts at 127 MHz for the carbon sites adjacent to the vacancy and decreases with the distance [354].

The most important terms in the ground-state Hamiltonian of the NV defect are therefore

$$\mathcal{H} = D\,S_z^2 + \mu_0 g \vec{B}\cdot\vec{S} + A_N \vec{S}\cdot\vec{I}_N + \sum_k A_C^k \vec{S}\cdot\vec{I}_C^k,$$

where the sum runs over all sites occupied by ^{13}C isotopes.

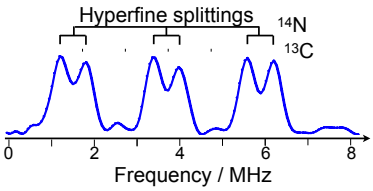

Figure 12.28: Spectrum from a single N/V center showing resolved hyperfine couplings to the ^{14}N and one ^{13}C nuclear spin.

Figure 12.28 shows a typical spectrum, obtained as the Fourier-transform of a free-induction decay. The $m_S = 0 \rightarrow m_S = -1$ transition of the electron spin is split by the hyperfine interaction with the ^{14}N nuclear spin ($A_N = 2.17$ MHz) and one ^{13}C nuclear spin ($A_C = 0.58$ MHz). Many additional nuclear spins couple to the electron spin with hyperfine coupling constants <= 0.3 MHz, which do not lead to resolved splittings, but to a broadening of the resonance line.

12.3.4 Quantum memory

The decay of electron spin coherence by the hyperfine interaction with the ^{13}C nuclear spins can be refocused by the usual spin-echo experiments. As shown in Fig. 12.29, a single refocusing pulse, corresponding to the Hahn echo, can generate echoes for delays of up to 10 μs. For longer times, the refocusing does not work, because fluctuations in the environment make the refocusing inefficient. Like in the case of molecular diffusion, it becomes then necessary to apply multiple refocusing pulses with shorter delays between them [123, 124]. As shown by the other curves in Fig. 12.29, sequences of refocusing pulses can extend the coherence time up to about 1 ms.

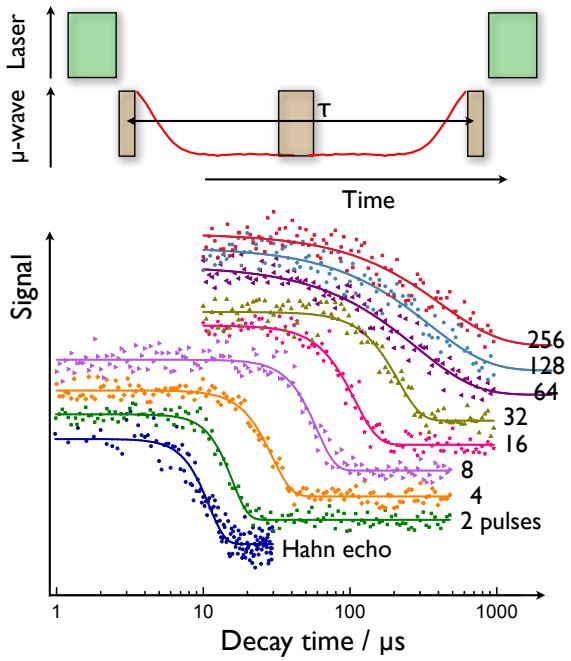

Figure 12.29: Refocusing of electron spin coherence by spin-echo experiments. The curves in the lower panel show the decay of the echo amplitude as a function of the total measurement time for different experiments with increasing number of refocusing pulses.

The experimental data of Fig. 12.29 show that the echo decay is not exponential. The curves drawn through the experimental points were obtained by fitting a "stretched exponential" $e^{-(t/T_2)^\beta}$ to the experimental data. For small numbers of refocusing pulses, the exponent is close to 1, but it becomes smaller for larger number of pulses, indicating a complex dynamics in the environment. One contribution to this comes from the Larmor precession of the ^{13}C nuclear spins, which is synchronized by the microwave pulses applied to the electron spins.

At the start of the experiment, the laser pulse initializes the electron spin into the $m_S = 0$ state. In this state, the secular part $S_z I_z$ of the hyperfine interaction vanishes and the nuclear spin interacts only with the external magnetic field. The $\pi/2$ microwave pulse then puts the system into a superposition of the $m_S = 0$ and $m_S = 1$ states. If the electron is in the $m_S = 1$ state, the nuclear spins interact not only with the external magnetic field, but also experience an effective field from the electron spin. In general, this effective field has a different direction than the external magnetic field. Depending on its state, the nuclear spin therefore experiences different quantization axes. Accordingly, the microwave pulse creates not only a superposition of electron spins, but also a superposition of the nuclear spins, which evolves between the $\pi/2$ and π pulses. The refocusing pulse cannot completely refocus such a time-dependent environment and the echo amplitude decreases. However, this evolution of the environment is partly coherent, since the Larmor frequency is the same for all ^{13}C spins. The environment therefore refocuses after a Larmor period and if the electron spin refocusing pulse is applied at this particular time $\tau = 2\pi/\Omega_C$ (or a multiple thereof), the echo amplitude recovers [355, 201].

Apart from the NV center, several other color centers in diamond have been identified and characterized, such as the Si-vacancy or the Sn-vacancy. While they have not been studied as extensively (yet) as the NV center, they appear to have promising properties for some interesting quantum tasks. Possible advantages are the emission spectrum, the contrast or the decoherence times.

Defects with similar properties have also been identified in SiC [356], although they have not been equally well characterized as the NV defect in diamond.

12.3.5 Single-spin readout

A difficult task in all spin-based quantum computer concepts is the readout of the result. While some of the concepts try to simplify this task by coding the qubits in ensembles of spins, it would be preferable to be able to read out individual spin. Several successful single-spin measurements have been reported that were based

on optical readout [197, 196, 198, 199], or scanning tunneling microscopy [316, 318]. A number of different approaches have been proposed [357, 358, 359].

The optical readout of spin is based on the optical readout of electronic states, but the details are strongly system-dependent. Early optical readout experiments concentrated on excited triplet states. Since the lifetime of the individual triplet states differs, a resonance microwave field that exchanged populations between them can "short-circuit" the decay of long-lived states. If a laser drives a transition from the ground state to an excited singlet state, some of the molecules undergo inter-system crossing to the lower lying triplet state. Since its lifetime is rather long, molecules get trapped in this state, thus reducing the ground state population. The observed fluorescence is a measure of the ground state population.

Resonant irradiation of triplet transitions changes the fraction of spins in the electronic ground state and is therefore observed as an increase in the fluorescence. Optical detection of fluorescence has, e.g., made it possible to perform and observe quantum gates on individual electronic and nuclear spins in diamond, using optical excitation of a nitrogen-vacancy (N/V)-center [360, 200, 201, 361].

A first step to readout of single centers is to determine if the signal stems from a single center. This issue can be well demonstrated for the case of the diamond NV-center. Each of the bright spots in the right-hand part of Fig. 12.25 represents a single N/V center. While it is not possible to determine this from the image alone, which was taken by scanning confocal microscopy with a resolution of $\approx$ 300 nm, it is possible to estimate it from the observed count rate.

A much cleaner signature, however, is obtained by measuring the correlation function of the arrival times of the photons on the detector. If we measure the delays τ between the arrival times of individual photons, we find that the probability for detecting a second photon immediately after the first drops to zero for short times [362]. This is easy to understand by considering that after the emission of a photon, the center is in the ground state and cannot emit another photon until it has absorbed one.

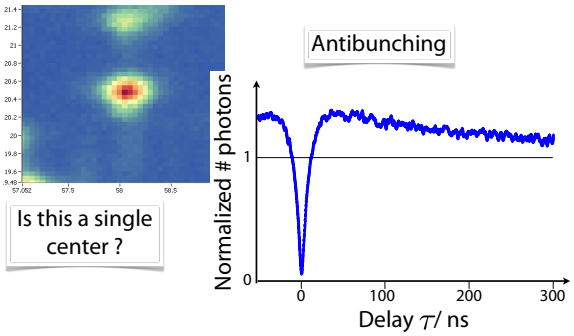

Figure 12.30: Photon correlation function for a single N/V center.

Fig. 12.30 shows an example: the emission rate drops almost to zero for short delays, and it takes $\approx$ 15 ns for the emission probability to rise again to its average value. This rise time decreases with increasing laser intensity.

12.3.6 Optimizing the readouot

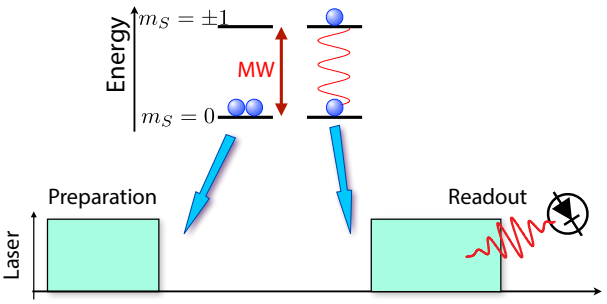

Figure 12.31: Basic sequence for time-resolved experiments.

Optical readout of the spin state is based on the different count rates emitted when the center is initially in a specific spin state. Figure 12.31 illustrates the principle: A first laser pulse initializes the spins into the $m_S = 0$ ground state. After the time-resolved experiment, typically driven by a sequence of microwave pulses,

the readout pulse measures the remaining population of the $m_S = 0$ state.

Since the laser also initializes the spin into the $m_S = 0$ state, this measurement is destructive, i.e. it changes the state, and the best results are obtained for a finite measurement time. If the system is initially in state $|0\rangle$, it scatters photons at a rate r_0. If it is initially in state $|\pm 1\rangle$, it scatters at rate $r_1 < r_0$. While scattering photons, it has a probability for changing to state $|0\rangle$, which can be quantified by a rate k. Accordingly, if the system is initially in state $|\pm 1\rangle$, the probability that it remains in this state decays as $p_1 = e^{-kt}$ and the population of state $|0\rangle$ increases as $p_0 = 1 - e^{-kt}$. Accordingly, the count rate increases as

$$r(t) = r_1 e^{-kt} + r_0(1 - e^{-kt}).$$

If we count photons for pulses of increasing duration τ, we expect to obtain

$$\begin{aligned} N_0(\tau) &= r_0\tau \qquad (12.3) \\ N_1(\tau) &= \int_0^\tau r(t)dt = r_0\tau - (r_0 - r_1)\frac{1 - e^{-k\tau}}{k} \end{aligned}$$

photons if the system is initially in state $|0\rangle$ or $|\pm 1\rangle$.

A simple procedure to determine the parameters is to determine r_0 by fitting N_0 vs. τ, and to determine k and r_1 by fitting

$$N_0(\tau) - N_1(\tau) = \frac{r_0 - r_1}{k}(1 - e^{-k\tau}).$$

As shown in figure 12.32, the difference signal $N_0(\tau) - N_1(\tau)$ increases monotonically with the duration τ of the counting period, but saturates for times $\tau \gg k^{-1}$. The shot noise, however, which is proportional to the total number $N_0(\tau) + N_1(\tau)$ of photons, increases without limit. Accordingly, the signal to noise ratio goes through a maximum for counting periods $\approx k^{-1}$. Typical numbers are $r_0 = 1.0 \cdot 10^5/\text{s}$, $r_1 = 0.80 \cdot 10^5/\text{s}$, and $k = 1.5\,\mu\text{s}^{-1} = 1/667\,\text{ns}$. With these numbers, the highest contrast to noise ratio is obtained for a pulse duration of

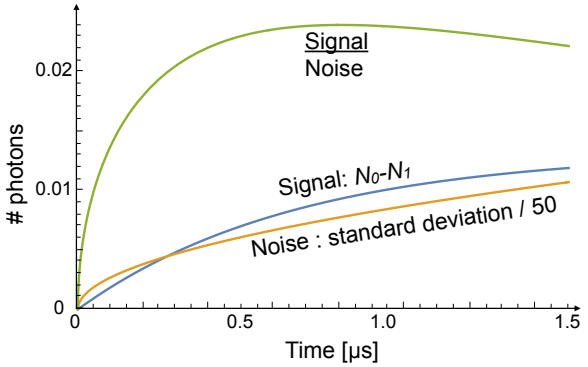

Figure 12.32: Number of detected photons during a single laser pulse as a function of the counting period. The noise is due to shot noise (Poissonian statistics). It has been divided by a factor of 50 to fit onto the same scale. The signal-to-noise ratio peaks for a counting period of approx. 0.8 µs.

838 ns. For shorter pulses, the number of detected photons is too small, for longer pulses, the spin has been reset into the $m_S = 0$ state and the additional counts contain no information. In practice, it is advantageous to count photons also during a later period, when the center is in the ground state. The ratio of the two count values is less sensitive to fluctuations of the laser intensity or drifts of the position of the microscope.

12.3.7 SiC, Si3N4

The properties of silicon carbide (SiC) are very similar to those of diamond. Its atomic structure is derived from that of diamond by replacing every second carbon by silicon. Since there are many nonequivalent variants of this structure, more than 200 polytypes have already been characterised.

Figure 12.33 shows a 2d projection of the structure of the 4H variant, including some typical spin centers like the silicon vacancy V_{Si}, the carbon vacancy V_C and some divacancies.

The many spin centers, which occur in different

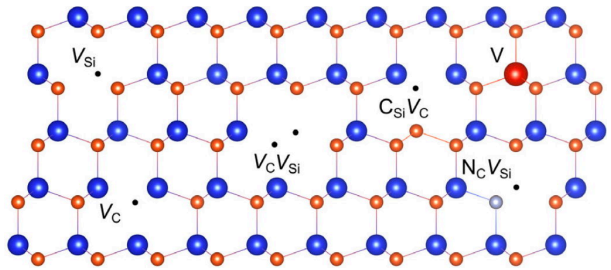

Figure 12.33: Structure of SiC with some typical spin centers.

polytypes, results in a wide range of properties. This makes it very interesting for developing applications like spin-photon entanglement [363]. Compared to diamond, it contains more nuclei with non-vanishing nuclear spin, which reduces the coherence time, unless isotopic purification is used. Under suitable conditions, the electron- as well as the nuclear spin can be read out in single-shot experiments [364].

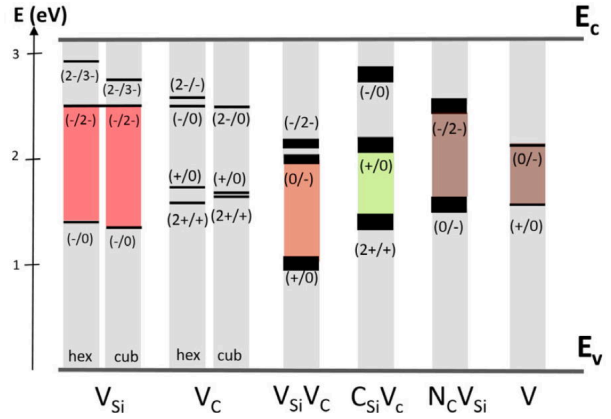

Figure 12.34: Energies of some spin centers within the bandgap of SiC.

Figure 12.34 shows the energy levels inside the band gap of the SiC host material for some of the centers that have been characterized so far. If the centers are to be used for converting qubits between spins and photons, it is often useful to have the photons emitted in the so-called telekom windows, where the absorption and/or dispersion are minimized.

12.4 Superconducting systems

Superconducting qubits are used by academic research groups (including USTC) as well as by industrial companies like Google, IBM, IMEC, BBN Technologies, Rigetti, Intel, and Baidu. Starting from very basic properties, this scheme has seen the fastest progress in the last 26 years.

12.4.1 Basics

Qubits can in principle be implemented as harmonic oscillators. If we consider an LC oscillator, it can be described classically by the differential equation

$$\frac{\partial^2 Q}{\partial t^2} + \frac{Q}{LC} = 0.$$

Quantum mechanically, this corresponds to the Hamiltonian

$$\mathcal{H} = \frac{\Phi^2}{2L} + \frac{Q^2}{2C} = \hbar\omega_0(n + \frac{1}{2}).$$

Qubits made from ordinary electrical circuits would decohere quickly owing to resistive power loss [365]. In superconductors at low temperature, however, electrons bind into Cooper pairs that condense into a state with zero-resistance current and a well-defined phase. In superconducting circuits, the potential for the quantum variables of that Cooper-pair condensate may be changed by controlling macroscopically defined inductances (L), capacitances (C), and so on, allowing the construction of qubits. Likewise, the potential may be dynamically altered by electrical signals to give complete quantum control. These devices therefore resemble classical high-speed integrated circuits and can be fabricated using existing technologies.

Typical parameters of these systems are dimensions on the order of $\approx 10\,\mu$m, inductances of 10^{-10}H, capacitance $C \approx 10^{-12}$F and resulting resonance frequencies $\omega_0 = \sqrt{1/LC} \approx 2\pi\,16\,$GHz. These parameters depend on the details of the manufacturing process. It is therefore important to control these parameters precisely, but also to analyze the actual devices and

calibrate the required control fields. For (near-)dissipation-free operation, the devices must be cooled to <50 mK in a dilution refrigerator. The thermal energy $k_B T$ must be small compared to the photon energy $\hbar\omega_0$, which again must be small compared to the gap energy Δ of the superconductor:

$$k_B T \ll \hbar\omega_0 \ll \Delta.$$

12.4.2 The Josephson effect

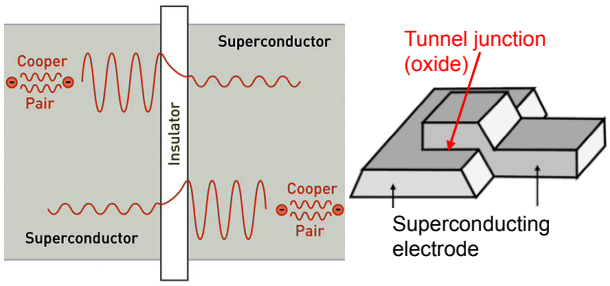

Figure 12.35: Josephson junction.

If 2 superconducting materials are separated by an insulating layer, as shown in figure 12.35, that layer is classically forbidden for the electrons and the Cooper pairs. However, if that layer is sufficiently thin, their wave functions can tunnel through that layer, effectively coupling the two reservoirs. This effect was predicted by Brian D. Josephson in 1962[2] and experimentally verified soon after. It is therefore known as Josephson effect and the arrangement as a Josephson contact. The current through this junction depends on the relative phase $\Delta\varphi$ between the wavefunctions in the superconducting materials as

$$I_J = I_c \sin \Delta\varphi,$$

where I_c is the critical current. In a magnetic field, the argument of the sin function depends also on the path integral of the vector potential $\vec{A}$ through the junction.

[2] At this time, Josephson was a 22-year old graduate student. He was awarded the Nobel prize in 1973, at the young age of 33 years.

For time-dependent voltages, the Josephson junction also represents an inductance L_J. Similar to the classical inductance, an energy

$$E(\varphi) = -E_J \cos\varphi$$

is associated with the current through the junction. The Josephson energy E_J is related to the inductance as

$$E_J = L_J I_c^2.$$

In this case, the energy is not related to the magnetic field density, but to the kinetic energy of the charge carriers.

12.4.3 Charge qubits

Superconducting materials owe their specific properties to a liquid formed by Cooper pairs, i.e., pairs of electrons held together by a coupling to lattice vibrations. The pairs have zero total spin and are therefore Bosons that can occupy a single quantum state subject to a simple effective Hamiltonian. As shown in Figure 12.36, typical qubit systems consist of a small "box" of superconducting material that is in contact with a reservoir of Cooper pairs through a Josephson junction (i.e., a thin layer of insulating material) [366].

The Coulomb energy required to bring a single electron with charge $-e$ onto a neutral qubit island is $\mathcal{E}_C = e^2/2C$, where C is the capacitance. Charging the island with n Cooper pairs requires an energy of

$$\mathcal{E}_C = \frac{(2ne)^2}{2C} = \frac{2n^2e^2}{C}.$$

In addition, a control electrode can change the electrostatic potential of the box. In this case, the energy becomes

$$\mathcal{E}_C = \frac{e^2}{2(C_g + C_J)},$$

where C_g and C_J are the capacitances to the control electrode and the reservoir. In addition to the mutual repulsion of the electrons,

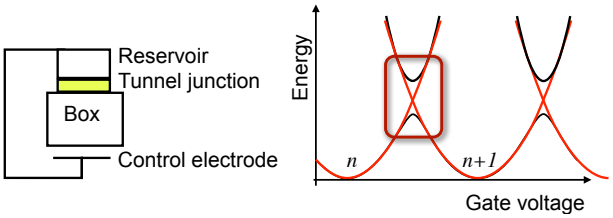

Figure 12.36: Components of a superconducting qubit (left) and its lowest energy levels as a function of the gate voltage (right).

the Coulomb energy depends on the potential applied through the control electrode. Since this energy contribution also depends on the net charge on the box, it is convenient to write the electrostatic part of the Hamiltonian as

$$\mathcal{H}_0 = 4E_C(n - n_g)^2, \tag{12.4}$$

where n is the number of excess Cooper pairs in the box[3] and $n_g = C_g V_g/2e$ parametrizes the control voltage. The control electrode therefore changes the number of excess Cooper pairs that makes the island effectively neutral.

The so-called charge qubits are defined by the number n of excess Cooper pairs on the island. Each n value yields one of the dashed parabolas in Figure 12.36, showing the quadratic dependence on the control voltage for each of the Cooper pair number eigenstates $|n\rangle$. These states are coupled by Cooper pair tunneling to the reservoir, represented by the Josephson coupling energy E_J. Choosing states $|n\rangle$ and $|n+1\rangle$ as the qubit states (and neglecting all other states), we can write an effective Hamiltonian for the qubit as

$$\mathcal{H} = 4\frac{E_C}{\hbar}(1 - 2n_g)\mathbf{S_z} - \frac{E_J}{\hbar}\mathbf{S_x}, \tag{12.5}$$

where we have shifted the origin of the energy axis to the mean of the two states. The pseudospin defined by the qubit therefore interacts with an adjustable magnetic field along its z-axis that is defined by the control electrode's potential, plus an effective field along the x-axis, which is determined by the Josephson splitting.

An obvious difficulty for this type of qubit is that the Hamiltonian is not diagonal in the chosen basis: the transverse field, which is determined by the tunnel splitting, cannot be switched off. The control voltage, which affects the longitudinal field, can be used to apply gates, but the qubits are never in a completely quiet state where the information does not evolve. A way to circumvent this problem was suggested by Makhlin *et al.* [367]: if the junction to the reservoir is replaced by a loop with two junctions, the magnetic flux through this loop can adjust the effective tunnel splitting.

12.4.4 Flux qubits

Rather than encoding the information in the charge degrees of freedom of small superconducting islands, it is also possible to associate the qubit states with two states of distinct magnetic flux through a superconducting ring [368]. Compared to the charge qubits, flux qubits should offer longer decoherence times, since they are not subject to electrostatic couplings to stray charges.

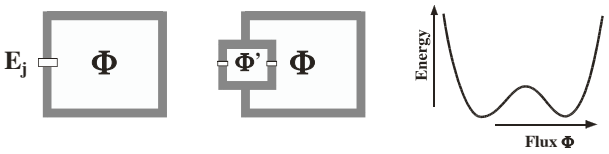

Figure 12.37: A simple flux qubit (left) consists of a loop that includes a Josephson junction. The second version allows control of the Josephson energy by the flux Φ'. The total energy forms a double well potential as a function of the flux.

Figure 12.37 shows the basic element of a flux qubit, a superconducting ring with a Josephson

[3] It is assumed that the box contains no unpaired conduction electrons. To suppress states with broken Cooper pairs, parameters can be chosen such that the superconducting energy gap Δ is the largest energy scale in the problem.

junction. The energy of the system is

$$\mathcal{H}_{\text{fl}} = -E_J \cos\left(2\pi\frac{\Phi}{\Phi_0}\right) + \frac{(\Phi-\Phi_x)^2}{2L} + \frac{Q^2}{2C_J},$$

where E_J is the Josephson energy, $\Phi_0 = h/2e$ is the flux quantum, Φ_x is an external flux bias, L the self-inductance of the loop, Q the charge, and C_J the capacitance of the junction. The first term represents the Josephson coupling energy of the junction, which is a periodic function of the flux Φ through the loop. The second term is the magnetic field energy of the flux, and the third the Coulomb energy of the charge over the junction.

For suitable parameters, the total energy forms a double well potential, as shown on the right-hand side of Figure 12.37. The two minima correspond to the two basis states of the flux qubit, which are coupled by the junction energy E_J. The longitudinal component of the effective magnetic field is now determined by the external flux, while the transverse component depends on the junction energy. In close analogy to the charge qubit, it is again possible to tune the junction energy by inserting a small loop and adjusting the flux through this control loop, as shown in the center of Figure 12.37.

12.4.5 Transmon and Unimon

Transmons are a special type of qubit with a shunted capacitor specifically designed to mitigate noise. It was based on the Cooper pair box and was the first qubit to demonstrate quantum supremacy. The increased ratio of Josephson to charge energy ($\mathcal{E}_J/\mathcal{E}_C \gg 1$) mitigates noise. To get long coherence times, they can be enclosed in superconducting resonators.

Two transmons can be coupled using a coupling capacitor. For this 2-qubit system the Hamiltonian is

$$\mathcal{H}_J = \frac{\hbar J}{2}(\sigma_1^x\sigma_2^x + \sigma_1^y\sigma_2^y).$$

Variants of this design are the Xmon, which is essentially a tunable transmon; its qubits are grounded with one of its capacitor pads. The Gatemon, another variant, is also tunable, via a gate voltage.

Another version was developed by IBM in 2022, called the Unimon. It consists of a single Josephson junction shunted by a linear inductor inside a (superconducting) resonator. Unimons have increased anharmonicity and display faster operation time resulting in lower susceptibility to noise.

12.4.6 Gate operations

As discussed above, the Hamiltonians that describe the charge as well as the flux qubits can be brought into the form of effective spin-1/2 systems, which are acted upon by effective magnetic fields. Depending on the details of the implementation, the components of this effective field can be changed over a certain range by suitable control parameters. Two different approaches have been used to implement gate operations: the control parameters can be switched between different values and left there at constant values for the suitable duration, or they can be modulated to resonantly excite a transition between the basis states.

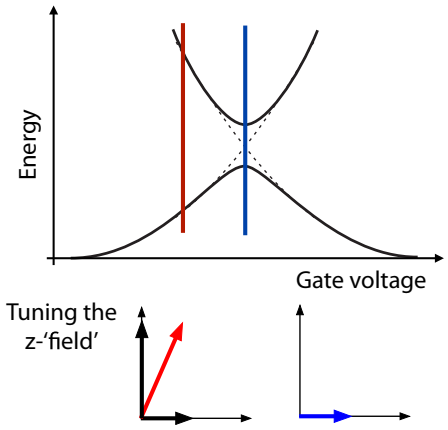

Figure 12.38: Gate operation for a charge qubit.

If dc (unmodulated) pulses are used, the whole process of switching the control field on, letting the system evolve, and switching back, should be

fast on the timescale of the unperturbed evolution of the system. With dc pulses, a coherent superposition of the two states can be created by initialization of the system into the ground state and then suddenly pulsing the control field to equalize the energy of the two states [369]. Leaving them in the degenerate states for a quarter of the tunneling cycle time creates an equal superposition of the two states. This superposition remains if the control field is switched off sufficiently rapidly.

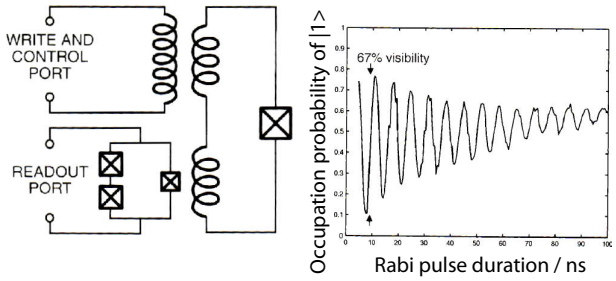

Figure 12.39: Resonant excitation of a superconducting qubit showing Rabi oscillations.

These very demanding requirements can be relaxed if resonant irradiation is used [370, 371]. The resulting evolution is then exactly that of a spin-1/2 under resonant irradiation.

12.4.7 Connecting Qubits

Like in any other implementation, two-qubit gates require a coupling between qubits. This can be implemented directly between qubits either through the Coulomb interaction between charges, which yields a coupling operator $\mathbf{S}_z^j \mathbf{S}_z^k$, in the basis of eq. (12.5), or through inductive coupling between flux states, which can be written in the form $\mathbf{S}_y^j \mathbf{S}_y^k$. For flux qubits, gate operations can be implemented by suitably time-dependent bias currents [372]: Such two-qubit gates were demonstrated by Yamamoto *et al.* [373], Berkley *et al.* [374], and by Plantenberg et al. [375].

For larger systems, it may be advantageous not to use pairwise couplings, but rather to couple each qubit to a common degree of freedom, such as an LC oscillator. The resulting system has a common "bus" qubit, in analogy to the trapped ions, where the motion is used as a common bus qubit. Such a procedure may simplify the coupling network and also lower the amount of decoherence introduced into the system by the gate electrodes.

Apart from the systems discussed here, superconducting qubits have also been implemented that are intermediate between the charge and flux qubit. Choosing such an intermediate state allows one to optimize, in particular, the decoherence by choosing the basis states such that the effects of external noise sources are minimized.

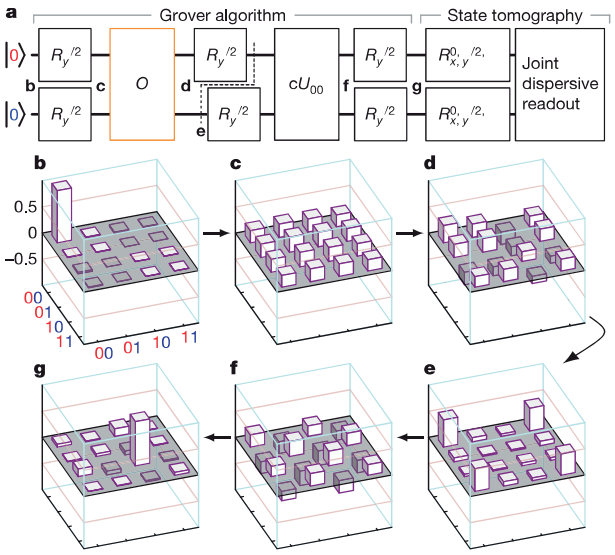

Figure 12.40: Grover algorithm implemented with 2 superconducting qubits.[376]

While early implementations of superconducting qubits had short coherence times and low fidelity quantum gate operations, multi-qubit systems are now possible that implement full quantum algorithms with useful fidelity. Fig. 12.40 shows, as an example, an implementation of Grover's algorithm using a pair of superconducting qubits [376].

12.4.8 Readout

In most cases, readout should convert the populations of the computational basis states into a measurable signal. For charge qubits, readout can be performed by an SET, which is very sensitive to small changes in the electric field. For flux qubits, SQUIDs (superconducting quantum interference devices) represent the most sensitive detection device. An early experiment [369] used a probe electrode that was coupled to the box by a tunnel junction, which provides an escape route for excess electrons in the box: if an excess Cooper pair is in the box, a tunnel current is registered through the probe gate. This electrode was also used to initialize the system into the ground state. In this experiment, the electrode was permanently coupled to the qubit box. The escape path for the electrons therefore presented a significant contribution to the decay of the coherence in the system. Since the coupling is an efficient source of decoherence for the system, it will have to be switched off for an actual quantum information processing device.

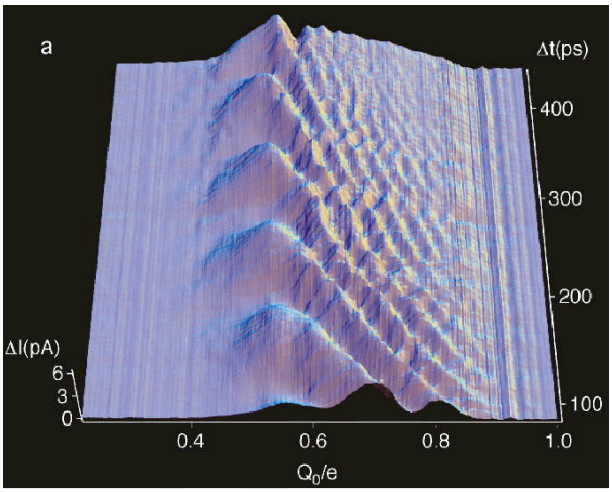

Figure 12.41: Signal from superconducting qubit undergoing Rabi oscillations as a function of control charge [369].

In the system displayed in Figure 12.41, Rabi oscillations have been initiated with an intense electrical field pulse. While the readout is done on a single system, it represents an average over a large number of pulse cycles. The measured quantity was therefore the probe current, not the number of electrons. It is proportional to the probability of finding the qubit in the upper state, from where electrons can tunnel out into the probe electrode. The oscillation period is given by the tunnel splitting, which can be tuned with the flux ϕ through the loop that includes the two tunnel junctions between the reservoir and the box. It agrees with the splitting that was measured by microwave spectroscopy. At larger offsets, the cycle Rabi frequency increases, but the oscillation amplitude decreases. To reduce noise, the experiment was performed at a temperature of 30 mK in a dilution refrigerator. Coherent dynamics of a single flux qubit have also been observed by [377].

While these readout schemes are destructive (i.e. they change the state of the qubit), it is also possible to read out the state nondestructively, using a dispersive coupling [378, 379]. In these schemes, the coupling between the qubit and the readout system is such that the readout circuit changes the frequency (or phase) of the qubit, but not the populations. These readout schemes can therefore be considered as quantum nondemolition measurements [179, 180].

12.4.9 Status of the field

After the first demonstrations of superconducting quantum bits, processors with up to 10 qubits became available around 2016. From then on, the number of qubits roughly doubled every year, with 127 qubits in 2021, 433 qubits in 2022, 1121 qubits in 2023. Possibly even more important is the fact that the quality of the operations has increased to a degree that suggests that robust processors are within reach [380][381]. At the same time, different groups have started to use these systems for potentially useful tasks like quantum machine learning or quantum chemical optimisations.

12.5 Semiconductor qubits

12.5.1 Materials

Semiconductor systems have been proposed very early for implementing quantum information processing [382]. One of their main attractions is that the technological requirements for building devices that are structured in the nanometer range have been extremely well developed by the semiconductor industry. Many of those technologies can be applied directly to QIP devices; no other material base has a similar range of tools available, not only for generating structures with dimensions in the nanometer range, but also for adjusting material properties like conductivity, potential, band-gap etc.

Semiconductor materials provide the richest set of tools for constructing qubits. Some of the proposed solid state spin based implementations use semiconductor materials in some form and were discussed in Section 12.1. Here we concentrate on other suggested systems that do not use impurity spins for the qubit implementation but use additional possibilities for defining qubits. This includes excitons, electron spins, nuclear spin, electric charges, and more. Most of these systems, however, have only been suggested as implementations and only a few, if any of them, are likely to be implemented for more than one qubit.

While the group IV materials Si and Ge were mostly used in implementations on the basis of impurity spins, III/V materials like GaAs are preferred for most of the other approaches. Using III/V materials is particularly important for implementations that use optical excitation or readout, which requires direct band-gap materials like GaAs. In addition, the high electron mobilities that can be reached in high-purity 2D electron systems, promise slow decoherence.

12.5.2 Quantum Dots

One possible basis for semiconductor qubits are quantum dots, i.e., structures that confine electrons in three dimensions in such a way that the energies become discrete. Typical sizes of these structures range from 5 to 50 nm.

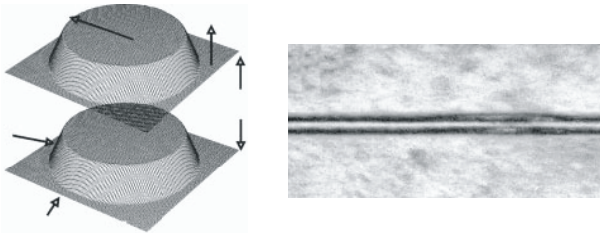

Figure 12.42: Two coupled quantum dots as qubits; left: schematic representation; right: transmission electron micrograph; height of dots is 1–2 nm, dot separation 4 nm, dot radius 8–12 nm [383, 384].

Quantum dots form spontaneously when some semiconductor materials are deposited on a substrate with a different lattice constant, e.g., during the growth of InAs on a GaAs substrate. The difference in lattice constant implies that the material grown on top is significantly strained. The elastic energy associated with this strain can be minimized if the layer grows not as a film, but assembles into islands; this process is called Stranski–Krastanow growth.

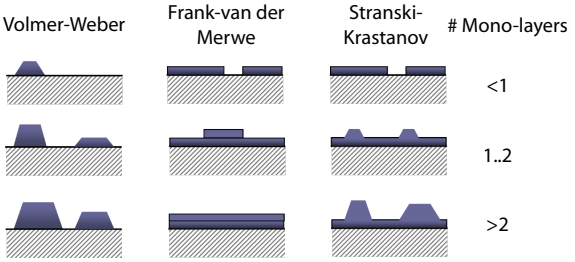

Figure 12.43: Growth modes of semiconductors during MBE.

Stopping the growth process at the right moment leaves an assembly of mesa-like structures behind, whose dimensions can be adjusted to match the range where quantum confinement effects are significant. If additional layers of GaAs and InAs are grown over the quantum dots, the dots in the second layer tend to align with the

existing dots. One has therefore a good chance to obtain coupled dots, as in the example shown in Figure 12.42.

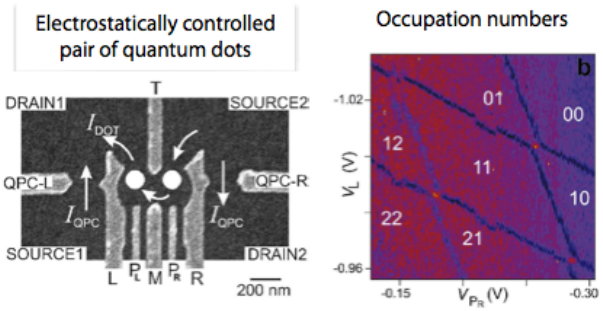

Figure 12.44: Electrostatically defined quantum dot pair. [385]

Quantum dots can also be defined electrostatically. By varying the electrostatic potential, it is then possible to define quantum states that correspond to different numbers of electrons in each quantum dot and use these states as computational basis states [385].

12.5.3 Excitons in quantum dots

The confinement of the electrons in the quantum dots makes the energy levels discrete, thus offering the possibility of using them for encoding quantum information. One possibility is to use excitonic states [386, 383], i.e., electron–hole pairs, which are created by the absorption of light. The energy $\mathcal{E}_{\text{ex}}$ of excitons is determined by $\mathcal{E}_{\text{ex}} = \mathcal{E}_g - \mathcal{E}_b$, where $\mathcal{E}_g$ is the band-gap and $\mathcal{E}_b$ the binding energy of the electron–hole pair.

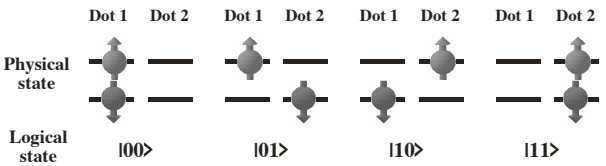

Figure 12.45: Possible encoding of two qubits by a single electron–hole pair in two quantum dots. State $|0\rangle$ is identified with the particle being in dot 1, state $|1\rangle$ with the particle in dot 2.

Using an exciton in a pair of coupled qubits, quantum information may be encoded into the electron and hole being in one or the other quantum dot: identifying the logical $|0\rangle$ with the left quantum dot, the four states shown in Figure 12.45 correspond to $|00\rangle$, $|10\rangle$, $|11\rangle$, and $|01\rangle$, respectively. At a separation of 4–8 nm, the electron wave-functions of the two quantum dots overlap, allowing electrons and holes to tunnel between them. The eigenstates are therefore the symmetric and antisymmetric linear combinations that are observed in the photoluminescence spectrum.

The excitons are usually generated by a short laser pulse. For single quantum dots, this process can be made coherent, as indicated by the observation of Rabi oscillations [387, 388]. Using the presence or absence of an exciton in a single quantum dot as the qubit, Bianucci et al. demonstrated a single-qubit Deutsch-Jozsa algorithm [171]. If two excitons are present in the same quantum dot, their interaction allows one to implement two qubits. Gates can again be performed by optical excitation, with different frequencies for the different transitions [389].

Readout of excitonic states is relatively straightforward in principle: the electron–hole pairs recombine after a time of the order of 1 ns [390], emitting a photon that can be detected. The wavelength of the photon indicates the state occupied by the particles before their decay. Depending on the coding scheme, the eigenstates of the system, which determine the photon wavelength, may not be the qubit states, but a modification of the algorithm could still make use of the information gained from the photoluminescence data. Unfortunately, the recombination destroys the quantum information stored in the exciton and the probability that the photon emitted by the electron–hole pair is subsequently detected is too low to allow for reliable readout in a single event. Instead of detecting an emitted photon, it is also possible to convert the photo-excited electrons into free carriers, which can then be detected electrically [388].

12.5.4 Electron spin qubits

Using the spin degree of freedom rather than the charge has two essential advantages. The Hilbert space consist only of the two spin states, thus minimizing any "leakage" of quantum information into other states. Second, while the lifetime of an exciton is limited by radiative recombination to ≈ 1 ns [390], observed spin lifetimes have increased from microseconds [391] to milliseconds [392].

Compared to nuclear spins, electron spins offer stronger couplings to magnetic fields and therefore faster gate operation, and they may be controlled by electric fields also [393]. The advantages of electron spins (fast gates) and nuclear spin (slow decoherence) may also be combined by storing the information in nuclear spin and switching it into electron spins for processing [394].

Specific spin states of electrons in quantum dots can be created either by optical excitation with circularly polarized light or by spin injection [395, 396, 397, 398] from magnetic materials. Manipulation of the spin states can be achieved either optically, by microwave pulses, or electrically. In the case of optical excitation, one uses Raman pulses that couple one of the qubit states to virtual states in the vicinity of trion[4] states [399, 400]. If the Raman laser field is kept well off-resonance, it creates only little excited state population and the associated decay rate remains small. Electrical excitation is possible if the quantum dot structures are defined by electrostatic potentials. Modulation of the potentials then modulates the tunnel splittings, which may be exploited for logical gate operations [401]. Coupling to the magnetic moment of the spin, it is also possible to drive the system by resonant microwave fields [402], in close analogy to NMR experiments.

The disadvantage of the III/V materials for spin-based qubits is that the natural abundance materials all have nuclear spins with which the electron spin interacts via the hyperfine interaction

$$\mathcal{H}_{hf} = S_z \sum_k A^k I_z^k,$$

where we have assumed that the electron spin is quantized in a strong magnetic field $\parallel z$. The sum runs over all nuclear spins I^k and the hyperfine coupling constant A^k is proportional to the electron density at the location of the corresponding nucleus. While the interaction of the individual nuclear spin with the electron is relatively weak, the number of interacting nuclei is very large. As a result, the combined interaction of the nuclear spins within the envelope of the electron wave function generates an effective magnetic field $B_N \approx \langle \sum_k A^k I_z^k \rangle$. This "nuclear field" adds to the Larmor precession of the electron spin with frequencies in the GHz range. Since the orientation of the nuclear spins is not constant in time, this effective field fluctuates and leads to a loss of coherence [403, 404] This is a much smaller problem in Si, where the most abundant species (^{28}Si) does not have a nuclear spin and therefore does not interact with the electron spin.

12.5.5 Readout

Readout of single electronic spins presents a significant challenge. Some of the solutions discussed in section 12.3.5 can be adapted to semiconductor-based systems. In addition, some other approaches have been suggested and a few of them have been implemented.

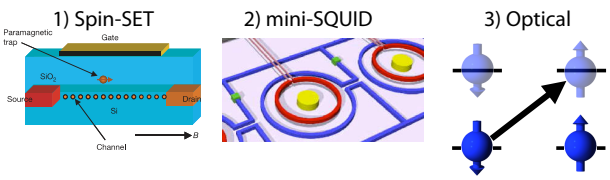

Figure 12.46: Some readout schemes for semiconductor-based qubits.

The approaches that are being investigated include optical readout, similar to the case of excitons, or electrical detection. In the case of optical

[4] A trion consists of an electron plus an exciton, i.e. two electrons and one hole in a bound state.

readout, the process can be amplified by driving a transition where, after excitation, the system falls back into the same initial state, thus allowing one to scatter many photons [405] and thus increasing the detection probability. However, in quantum dots, the number of photons that can be scattered in this manner is much smaller than for free atoms. Using dispersive optical detection, such as Kerr rotation measurements [406], it is again possible to minimize the disturbance of the electron spin.

Electrical readout of spin qubits can be performed by converting the spin state to a charge state and using single electron techniques for readout [407, 408]. The conversion into a charge state can be performed by spin-dependent tunneling. Like in superconducting systems, readout may be easier in intermediate systems that do not rely on individual spins, but on ensembles with pseudo-spin, such as "quantum hall droplets" [409].

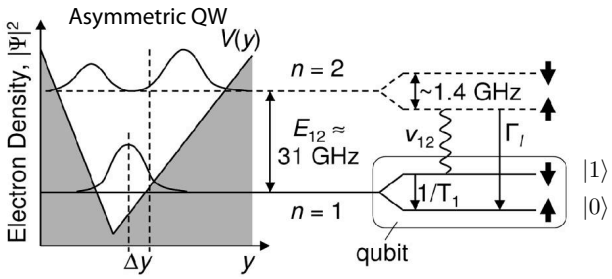

Figure 12.47: Readout scheme for a spin-qubit in an asymmetric quantum well.[410]

Friesen proposed a readout scheme for electron spin qubits in SiGe heterostructures [410]. In the asymmetric quantum well, an excitation of the electron from the ground state of the well to the first excited state shifts the charge laterally by an amount Δy. This change of the electric charge distribution can be detected, e.g., by a single electron transistor. The excitation can be driven resonantly, and since the frequency depends on the spin state, it can be made spin-selective.

12.6 Others

12.6.1 Majorana qubits

A Majorana fermion is a fermion that is its own antiparticle. They were hypothesised by Ettore Majorana in 1937. Quasiparticles with these properties are also hypothesized to exist in condensed matter physics: collective excitations may generate pairs of quasiparticles that have no charge and spin 1/2 and can annihilate each other.

In a superconductor, Majorana fermions can appear as excitations called Bogoliubov quasiparticles, which are their own antiparticles. They can be bound to a defect at zero energy, and then the combined objects are called Majorana bound states or Majorana zero modes. These objects are no longer fermionic but they are an example of non-Abelian anyons.

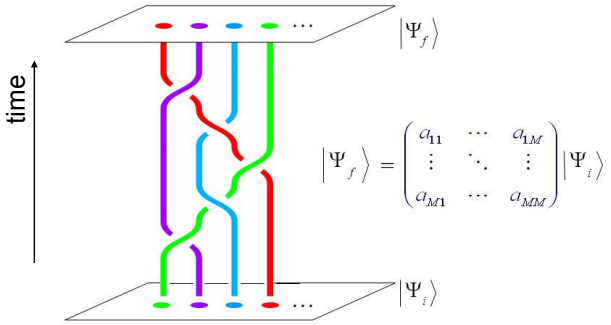

Figure 12.48: Braiding of anyons for topological quantum computing.

As shown in figure 12.48, anyons exist in 2-dimensional systems. Interchanging them changes the state of the system in a way that depends only on the order in which the exchange was performed. In the figure, the vertical axis represents time and the interchange of 2 quasiparticles is symbolized by the colored tubes extending from the initial state at the bottom to the final state on top. This process allows to use Majorana bound states as a building block for a topological quantum computer [411] [412, 413].

This approach is mostly pioneered by Microsoft. Their design incorporates superconducting-

semiconductor heterostructures, quantum dots for measurement control, and microwave readout systems capable of low-error measurements. This design should should be scalable to large systems [414]. However, the results published up to 2025 are not yet sufficiently convincing that this can be considered a viable technology.